Antimicrobial properties of Cu-based bulk metallic glass composites after surface modification

Victor M. Villapún[a]

S. Tardío[b]

P. Cumpson[b]

J.G. Burgess[c]

L.G. Dover[d]

S. González[a, *]

sergio.sanchez@northumbria.ac.uk

[a]Faculty of Engineering and Environment, Northumbria University, Newcastle upon Tyne, NE1 8ST, UK

[b]School of Mechanical and Systems Engineering, Newcastle University, Newcastle upon Tyne, Tyne and Wear, NE1 7RU, UK

[c]School of Natural and Environmental Sciences, Newcastle University, Newcastle upon Tyne, Tyne and Wear, NE1 7RU, UK

[d]Faculty of Health and Life Sciences, Northumbria University, Newcastle upon Tyne, NE1 8ST, UK

*Corresponding author.

Abstract

The aim of this work is to study the influence of two surface modification methods, surface grinding to change the surface roughness (from 240 to 4000 grit) and oxidation (furnace at 703 K for 5 h in air), on antibacterial activity against *E. coli K12* of a Cu-based bulk metallic glass composite (BMGC). Variations of roughness obtained through grinding in both as-cast and oxidized samples had a minimal effect on antimicrobial activity. Oxidation in resulted in a multilayered structure with an outer CuO layer, followed by Cu_2O layer and other phases at greater depths according to microscopy and energy dispersive X-ray results. This oxidation increased antimicrobial performance despite the CuO layer is poorer in copper than the $Cu_{55}Zr_{40}Al_5$ at. % bulk metallic glass composite substrate. This improvement could be attributed to microstructural differences between the layer and the substrate. The fine needle-shape structure of the crystalline oxide layer may account for the improvement since interphase boundaries could constitute easy diffusion paths for Cu ion release while the shape could trigger mechanosensitive channels that can favour and thus promote the migration of copper ions into the cell. Microscopy of the deposited bacteria revealed limited changes of the outer layer of the cells, with slight changes in morphology for the oxidized samples and this is attributed to the higher copper ion released. Minimum Inhibitory Concentration tests revealed that cell degradation takes place at copper concentrations of 222.4 mg/mL, much higher than measurements of copper ion diffusion in the as-cast samples, suggesting that lysis is not the first step in copper ion toxicity. These studies indicate that $Cu_{55}Zr_{40}Al_5$ bulk metallic glass composite shows promise as an antimicrobial material with tuned performance through surface oxidation.

Keywords: Antimicrobial properties; Metallic glass composite; Roughness; Oxidation

~~1.~~1 Introduction

Healthcare-associated Infections (HCAIs) are infections that can arise either through being in contact with a healthcare setting or through medical or surgical interventions. Increasing antibiotic resistance of hospital pathogens and the emergence of multi-drug resistant bacteria able to tolerate the last-resort antibiotic (colistin) is a serious threat [1]. Thus, strategies that can reduce the probability of infection in hospitals, without the use of antibiotics are urgently needed. In this regard, the use of antimicrobial surfaces is an efficient strategy to prevent the spread of infections. This is notably relevant in hospitals where surfaces that become a reservoir of pathogens can cause patient infections and even patient death. In addition, HCAIs result in substantial economic losses [2].

Of all antimicrobial materials, copper is a well-known material for its antibacterial properties, although its use in hospitals has been limited partly because of its poor wear performance. In this regard, Cu-rich bulk metallic glass composites (BMGCs) are interesting materials since it is possible to tune their antimicrobial and wear performance by controlling the composition and the volume fraction of the amorphous/crystalline phase [3]. In addition, when containing high enough concentrations of Cu (at least about 30 at. % Cu), the alloys exhibit antimicrobial behavior against the Gram positive pathogen *Staphylococcus aureus* [4] which is attributed to the release of copper ions. For Cu ions to diffuse effectively, the presence of diffusion paths needs to be favored, and this can be attained by promoting the presence of a large volume fraction of Cu-rich crystalline phases due to the large concentration of Cu and the large volume fraction of interphase boundaries [3,5].

However, high concentrations of Cu can be detrimental for applications where the alloy is subjected to wear because it is a soft metal [6]. One strategy to increase the wear resistance of Cu-rich alloys is to promote the formation of Cu oxides at the surface since they are more wear resistant than pure Cu. However, to achieve this, a relatively high concentration of Cu is required, especially when in the presence of elements with a high affinity for oxygen such as Zr [7]. The formation Cu oxide scale on the surface may result in a decrease in antimicrobial performance due to Cu depletion of the scale compared to a pure Cu substrate. This was observed by Hans et al. [8] when studying the contact killing effect of pure Cu (in rolled sheet form) and Cu oxides on *Enterococcus hirae*. Their results revealed that the highest antimicrobial activity was observed for pure Cu, followed by Cu_2O and finally CuO. Although there is plenty of literature about the antibacterial activity of copper oxide and other metal oxides in the form of nanoparticles [9,10], information when copper oxides are in bulk shape [8] is very scarce. Even the size of the nanoparticles can have an effect on the antimicrobial performance [1,11] and therefore this parameter has to be taken into consideration. Another important physical parameter that can influence antimicrobial performance is surface roughness [12] since this can also have an effect on the wettability [13] and therefore on the bacteria-surface attachment. The effect of surfaces of various geometries (pillars, hexagons, etc.) with controlled parameters (height, width and spacing) on bacterial attachment has been studied over the years [12]. These features have a nanometer to micron size range, similar to the size of bacterial cells and therefore, they should have an effect on bacterial attachment. However, despite the potential interest of the surface roughness generated upon grinding on the antimicrobial properties, it has not been studied before. In this work, we have explored whether the combined effect of roughness and oxidation can enhance the antimicrobial performance of copper containing BMGCs. The contact killing efficiency of copper oxide coatings with different roughness was studied using *Escherichia coli* in wet conditions.

2.2 Materials and methods

Alloy ingots with a nominal composition of $Cu_{55}Zr_{40}Al_5$ at. % were prepared from elements with purity higher than 99.9 at. %. The master alloys were re-melted three times to attain good chemical homogeneity in a high purity argon atmosphere with two different getters (Zr and Ti). Rod samples of 2 mm diameter were prepared from the master alloy by copper mold casting in an inert argon gas atmosphere and 10 litre/min flow rate. Suction casting was done once the master alloy reached the melting temperature (starts to glow red). The composition of the samples was checked by SEM-EDX, and it is the average value of 3 measurements (3 areas from the sample of about 1 mm x × 1 mm).

The surface roughness of the samples were was mechanically ground with SiC paper (grit 250, 1200 and 4000). To form the oxide layers, some of these samples were oxidized at 703 K for 5 h and left to cool to room temperature. The structure was studied by X-ray diffraction (XRD) using a Bruker D8 diffractometer with monochromatic Cu Kα_radiation (2θ range 20°-90°, step size = 0.03°). The microstructure was investigated by Scanning Electron Microscopy (SEM). X-ray Photoelectron Spectroscopy (XPS) analyses were carried out on a K-Alpha (Thermo Scientific) instrument using Al Ka radiation (1486.6 eV), measuring directly from the surface and after sputtering the surface of the thermally treated samples with Ar ions for 180 s with an energy of 4 keV. All spectral positions were charge corrected taking C 1 s peak at 285 eV. The roughness and profile were analyzed using an Alicona profilometer and the profiles were obtained averaging 5 measurements.

The antibacterial activity of the alloys was assessed by following changes in the recovered colony forming units (CFU) from the surface over time (Fig. 1) [3]. *Escherichia coli* strain K12 (Gram-negative) was incubated in an orbital incubator (37 °C, 180 rpm), in 25 mL of LB (Luria-Bertani) broth for 16 h. Culture yield was quantified by measuring optical density (OD_{600}). To prevent aggregation and to provide the most sensitive preparation with no dead cells that might absorb Cu ions, the bacteria were diluted in sterile LB Broth to an optical density of 0.01 and cultivated at 37 °C until they reached an OD_{600} ~ 0.3. Metallic glass samples and control samples (stainless steel 314) were immersed in 100 % ethanol and sonicated for 5 min in an ultrasound bath to ensure a clean and disinfected surface. After drying in a sterile petri dish, these samples were placed inside a sterile petri dish containing tissue paper wetted with 1 mL of sterile LB Broth to prevent sample drying. The inoculum (2 μL) was dispensed directly onto the surfaces (as-cast and oxidized 4000 grit) and control (stainless steel) and incubated at room temperature in the sealed containers. After the designated exposure time, the samples were diluted in 198 μL of Tween 20 0.148 g/L (2 × CMC) and sonicated for 5 min. Finally, the recovered bacterial suspension was subject to serial decimal dilution, plated onto LB agar plates and the resulting colonies were counted after 16 h of incubation at 37 °C. All tests were performed five times, with mean counts and standard deviation reported.

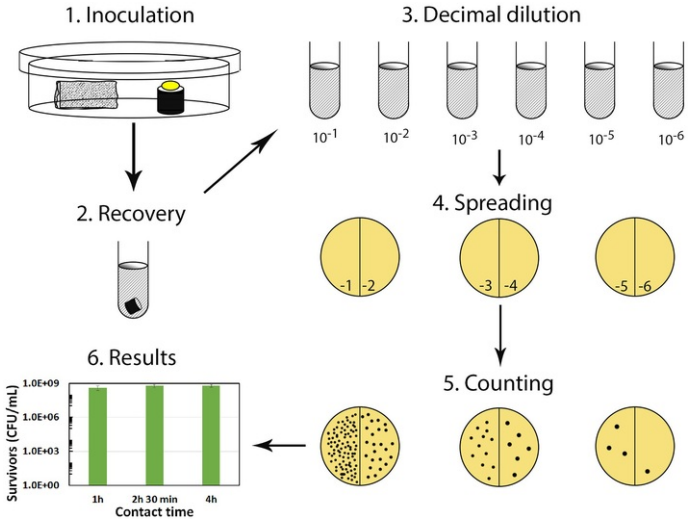

~~Fig. 1.~~Fig. 1 Schematic diagram showing the antimicrobial tests.

alt-text: Fig. 1

Minimum Inhibitory Concentration (MIC) tests were developed following the Clinical & Laboratory Standards Institute (CLSI) M07-A9 standard [14]. An initial dissolution of 10 mM of copper (II) chloride dihydrate ($CuCl_2 \cdot 2(H_2O)$) in LB broth was prepared. This solution was diluted in sterile LB broth to obtain serial dilutions from 0 to 5 mM in 0.5 mM steps in sterile 13~~x~~×100 mm test tubes. *E. coli K12* colonies from a fresh (18–24 hour post inoculation) agar plate were suspended in LB broth and cultivated in an orbital incubator (180 rpm) overnight. The turbidity of these cultures was adjusted using a 0.5 McFarland standard and then were diluted 1:150 in LB broth to a final culture density of ~5~~x~~×10^5 CFU/mL. During the next 15~~ minutes~~min after the dilution, 2.5 mL of inoculum was introduced into 2.5 mL of the corresponding $CuCl_2 \cdot 2(H_2O)$ dilutions. Tubes of pure inoculum and 100 µL of 1:1000 dilution of inoculum were plated in LB agar to check the purity of the sampled bacteria. All tests were done in triplicate and incubated at 37 °C overnight.

Scanning Electron Microscopy (SEM) images of deposited bacteria were performed using a variation of the method described by Fisher et al. [15]. Inoculum preparation and disinfection of the samples was done as described in the antibacterial tests. 2 µL of inoculum were deposited on the samples and left for up to 4 h into a sterile petri dish with a wetted cloth with 1 mL of LB broth. After the designated contact time, samples were moved into different 24 well plates and 1 mL of 2.5 % glutaraldehyde was dispersed against the wall of the well to regulate the flow across the samples. After 1 h, samples were washed with phosphate-buffered saline (PBS) three times for 2 min each. A graded ethanol series (25 %, 50 %, 75 % and 95 %, v/v) was used to dehydrate the samples; 1 mL of each dilution was applied for 5 min, and introduced in pure ethanol for 10 min. After drying, samples were coated with 2–3 nm of platinum using a Q150R Rotary-Pumped Sputter Coater (Quorum Technologies).

To measure the number of copper ions released from the samples, 2 µL of LB broth were deposited on 4000 grit as-cast and oxidized samples. All samples were disinfected and degreased using the same protocol described in the antimicrobial test and placed into a sterile petri dish with a wetted cloth. After 1, 2.5 and 4 h, samples were recovered and introduced into a cleaned and disinfected universal containing 10.0 mL of deionized water from a Milli-DI purification system. Samples were sonicated for 5 min and BMG composites were subsequently recovered. Dilutions were processed using Inductively Coupled Plasma spectrometry (PerkinElmer Optima 8000 ICP-OES). All tests were done four times with mean counts and standard deviation reported.

~~3.~~3 Results and discussion

~~3.1.~~3.1 Microstructure and oxide characterization

Fig. 2 shows the XRD scans for $Cu_{55}Zr_{40}Al_5$ alloy in the as-cast and oxidized (air at 703 K for 5 h) conditions (Fig. 2a), along with their corresponding SEM images for the former (Fig. 2b) and last conditions (Fig. 2c), respectively. For the as-cast sample, high intensity XRD peaks overlap to an amorphous hump thus suggesting the presence of both crystalline and amorphous phases. The peaks can be associated to orthorhombic $Cu_{10}Zr_7$ (a = 0.9347 nm, b = 0.9347 nm, c = 1.2675 nm), orthorhombic Cu_8Zr_3 (a = 0.78686 nm, b = 0.81467 nm, c = 0.9977 nm), austenite B2 CuZr (a = 3.2562 nm, b = 3.2562 nm, c = 3.2562 nm), monoclinic martensite B19′ CuZr (a = 0.3237 nm, b = 0.4138 nm, c = 0.5449 nm) and tetragonal $CuZr_2$ (a = 0.3220 nm, b = 0.3220 nm, c = 1.1183 nm). For the oxidized samples, along with the peaks corresponding to the phases described for the as-cast samples, additional peaks matching monoclinic

CuO (a = 0.4653 nm, b = 0.3410 nm, c = 0.5108 nm), cubic Cu_2O (a = 0.4252 nm, b = 0.4252 nm, c = 0.4252 nm), tetragonal ZrO_2 (a = 0.5070 nm, b = 0.5070 nm, c = 0.5160 nm) and face-centered cubic Cu (a = 0.3608 nm, b = 0.3608 nm, c = 0.3608 nm) were detected.

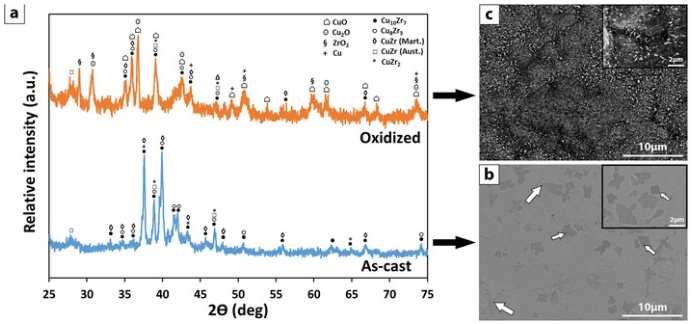

~~Fig. 2.~~Fig. 2 (a) XRD scans for $Cu_{55}Zr_{40}Al_5$ BMGC in the as-cast and oxidized (air at 703 K for 5 h) conditions along the corresponding SEM backscattered images for the surfaces of the (b) as-cast and (c) oxidized samples.

alt-text: Fig. 2

The backscattered SEM image for the as-cast sample (Fig. 2b) shows particles of cubic (small arrows) and dendritic (large arrows) shape of up to 5 μm in size embedded in a featureless matrix, which is distinctive of the amorphous nature of the matrix. According to EDX analysis the composition of the cubic particles is $Cu_{36.2}Zr_{51.0}Al_{12.8}$ (at. %) and therefore could be attributed to $CuZr_2$, while the dendritic particles have a composition relatively poorer in Zr, $Cu_{46.3}Zr_{41.1}Al_{4.7}$ (at. %) and could correspond to CuZr. The composition of the matrix far from the crystalline phases was, as expected, the same as the nominal composition. When the sample was oxidized at 703 K for 5 h (Fig. 2c), the microstructure changes dramatically. It consists of granules of similar morphology to those observed for $Cu_{60}Zr_{30}Ti_{10}$ at. % oxidized at 573 K [16] but for our sample the granules are coarser (≈5 μm), probably due to the higher oxidation temperature. Also, small needle shaped crystalline phases of about 1 μm size of white tonality can be detected in the backscattered magnified image (inset of Fig. 2c) of the oxidized sample and therefore it might be attributed to an oxide.

In order to quantify the roughness of the various samples after being ground with SiC abrasive grinding paper of 240, 1200 and 4000 grit size and the influence of oxidation on the sample roughness, the ground samples were subsequently oxidized at 703 K for 5 h and all the surfaces analyzed using a profilometer (Fig. 3). The average roughness values measured perpendicular to the grinding direction are: $R_a = 430.9 \pm 33.4$ nm (240 grit), $R_a = 606.8 \pm 88.9$ nm (240 grit and oxidized), $R_a = 216.0 \pm 12.2$ nm (1200 grit), $R_a = 484.8 \pm 46.5$ nm (1200 grit and oxidized), $R_a = 68.8 \pm 11.9$ nm (4000 grit) and $R_a = 274.3 \pm 24.1$ nm (4000 grit and oxidized). The roughness values are always larger after oxidation. These results clearly showed that oxidation increases the surface roughness in all cases and that the effect is more pronounced as the grit size decreases: ~4 times rougher for 4000 grit, ~2.2 times rougher for 1200 grit and ~1.4 times rougher for 240 grit.

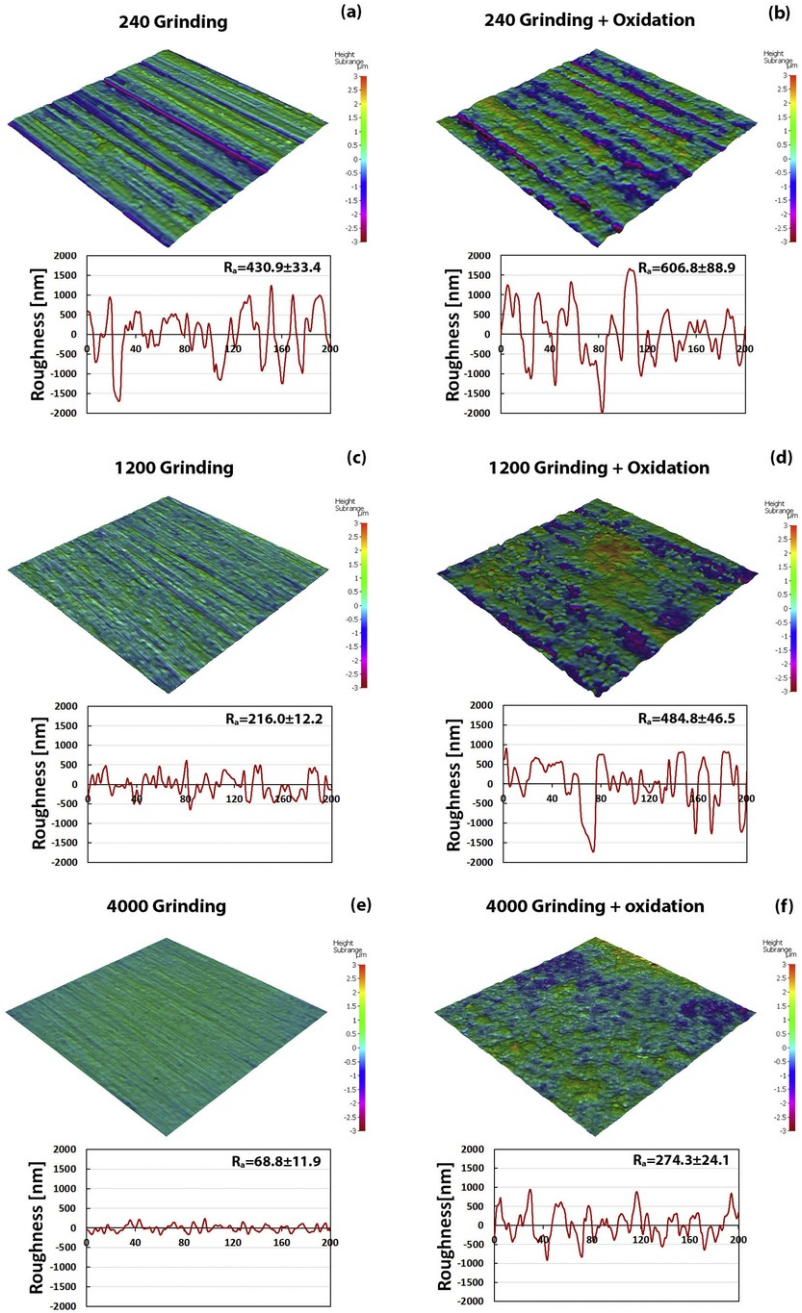

~~Fig. 3.~~ Fig. 3 Surface topography for different surface roughness (250, 1200, and 4000 grit) before and after oxidation.

alt-text: Fig. 3

To better understand the nature of the oxide scale formed, a cross section of the sample prepared with 240 grit SiC was observed under the SEM (Fig. 4). Secondary electron image (Fig. 4a) showed an intermediate porous layer below the outer layer. In addition, several oxide layers of different tonality of up to 13 μm thickness can be appreciated from the backscattered image of Fig. 4b, suggesting that their compositions are different. To identify the composition of each layer, elemental EDX mapping images Fig. 4c have been obtained. The results show Al-rich (green), Cu-rich (blue), Zr-rich (red) and O-rich (orange) regions. The mapping shows a maximum oxygen content at the outermost part of the coating, which decreased with increasing distance from the surface. These results are consistent with the natural progressive formation of oxides. According to the EDX analysis, the composition of the outmost oxide layer of darkest tonality and up to 0.7 μm thick is $Cu_{51.1}O_{49.9}$ (at. %), which can be attributed to CuO. The composition of the second layer of brighter tonality (see arrow) is $Cu_{68.2}O_{31.8}$ at. % and therefore could be assigned as Cu_2O. The third layer is discontinuous and consists of a mixture of Cu oxides and pure copper. The innermost layer, however, mostly consists of Zr_2O, with some traces of Cu and Al, according to the EDX results ($O_{54.0}Zr_{26.9}Cu_{15.8}Al_{3.4}$ at. %.). These EDX analysis are consistent with the SEM mappings. In addition, similar observations have been reported by other authors [17] explaining the multi-layered structure of Cu-Zr oxides through the preferential oxidation of Zr to form ZrO_2. Firstly, a protective ZrO_2 layer will be formed. The pores and other defects present in this layer will make possible the diffusion of oxygen into the alloy, thus resulting in further oxidation of Zr. The observations of this multi-layered oxide film agrees with the results from Tam et al. [16,18] for other Cu-rich BMGs, while González et al. have shown complex oxide layers in the Zr-Cu-Al-Fe system [7].

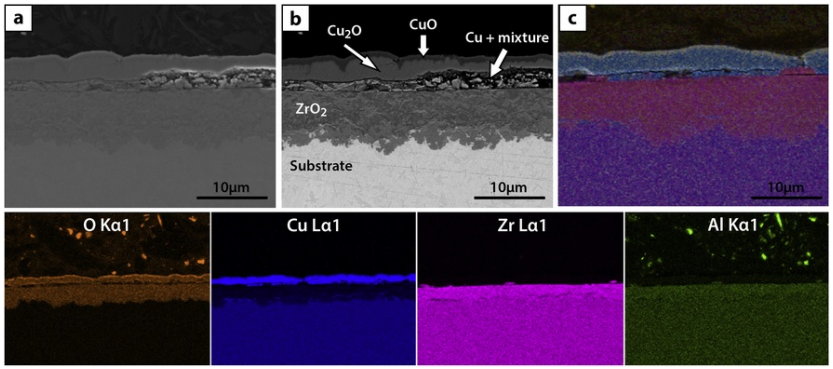

~~Fig. 4.~~Fig. 4 a) Secondary electron and b) backscattered SEM images for the transversal section of the 240 grit SiC oxide coating. Compositional X-ray mappings corresponding to Cu, Zr, O and Al.

alt-text: Fig. 4

To further characterise the oxide layer, XPS analyses were carried out measuring directly from the surface (Fig. 5a) and after argon ion sputtering for 180 s with an energy of 4 keV (Fig. 5b). The survey spectra of both measurements indicate the presence of O, Cu, Zr and Al elements with small amounts of C, N and Si from surface contamination. The intensity of these latter peak decreases in the spectra obtained after sputtering. The relative concentration of the metals detected shows that the stoichiometry of the material at the unsputtered surface is different from the nominal one with higher amount of Zr. Additionally, the copper concentration measured was greater at the native surface than after sputtering. This seems to suggest the presence of a layered structure, with the copper rich oxide layer above a thicker, Zr-rich oxide layer consistent with the data obtained via EDX illustrated in Fig. 4.

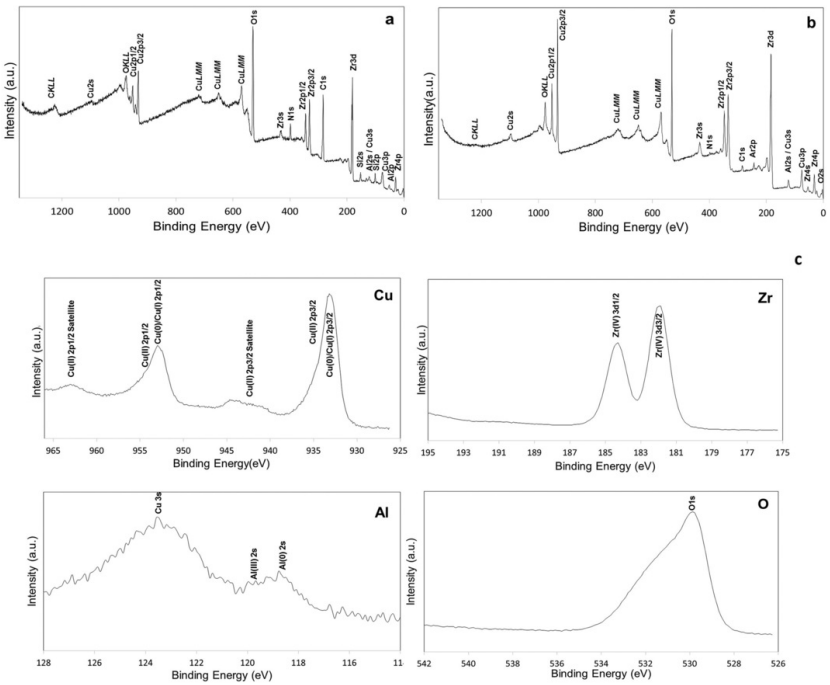

~~Fig. 5.~~Fig. 5 XPS survey spectra of the oxide layer formed by air-annealing at 703 K for 5 h of $Cu_{55}Zr_{40}Al_5$. a) From the surface and b) after sputtering for 180s. Cu 2p, Zr 3d, Al 2s and O 1s core-level XPS spectra c) from the surface of the oxide layer (unsputtered) are also shown.

alt-text: Fig. 5

A summary of the oxidation states of the metal at the surface (before sputtering) is presented in Fig. 5c and shows Cu 2p, Zr 3d, Al 2s and O 1s high resolution spectra from the surface. The Cu 2p peak (which splits into 2p 3/2 and 2p½ components, at 931.8 eV and 951.6 eV, respectively) is mainly compatible with Cu^{+1} and the zero valence state of elemental Cu, although the presence of a small satellite below 945 eV together with the asymmetry of the peaks, suggests the presence of a small amounts of Cu (II).

The Zr 3d5/2 and 3d3/2 doublet are located at 182.0 and 184.3 eV, respectively, which matches the Zr^{4+} valence state. The Al 2s peak seems consist of two chemically shifted; Al(0) (118.8 eV) and Al(III) (119.9 eV). The O 1s peak is due to the metal oxides (on the low binding energy side) and components likely caused by the surface contaminants and metal hydroxide (e.g. C

O, C

O, M-OH etc.) on the higher binding energy side.

~~3.2.~~3.2 Antimicrobial performance and MIC

In order to analyze the antimicrobial behavior of the as-cast and oxidized $Cu_{55}Zr_{40}Al_5$ alloy, the recovery of *E. coli* colony forming units (CFU) from the sample surface after 1, 2.5 and 4 h contact time was measured (Fig. 6). As previously shown, surface oxidation results in an increase of surface roughness (Fig. 3) and therefore, in order to separate the effect of roughness from the effect of oxidation, survival rate values for the non-oxidized samples ground with 240, 1200 and 4000 grit size were also studied. These results were compared with type 314 stainless steel coupons as control sample for which an almost constant recovery of CFU (~5~~x~~ × 10^8 CFU/mL) with up to 4 h contact was observed, thus indicating that there is no external factor affecting the antimicrobial performance. The antimicrobial behavior has been additionally studied from the surface morphology of bacteria. Representative SEM images of *E. coli* after 4 h of contact with the surface of stainless steel coupons (Fig. 6a) and the 4000 ground samples before (Fig. 6b) and after oxidation (Fig. 6c) are shown. Survival rate graphs are the result of a statistical analysis of the antimicrobial performance using 4 samples. Considering that previous studies comment about the possibility to correlate the subtle morphological changes to the outer membrane with a reduction in viable cells [19,20], representative SEM images of bacteria deposited on different surfaces have been ~~analysed~~analyzed in this study (Figs. 6 a, b and c).

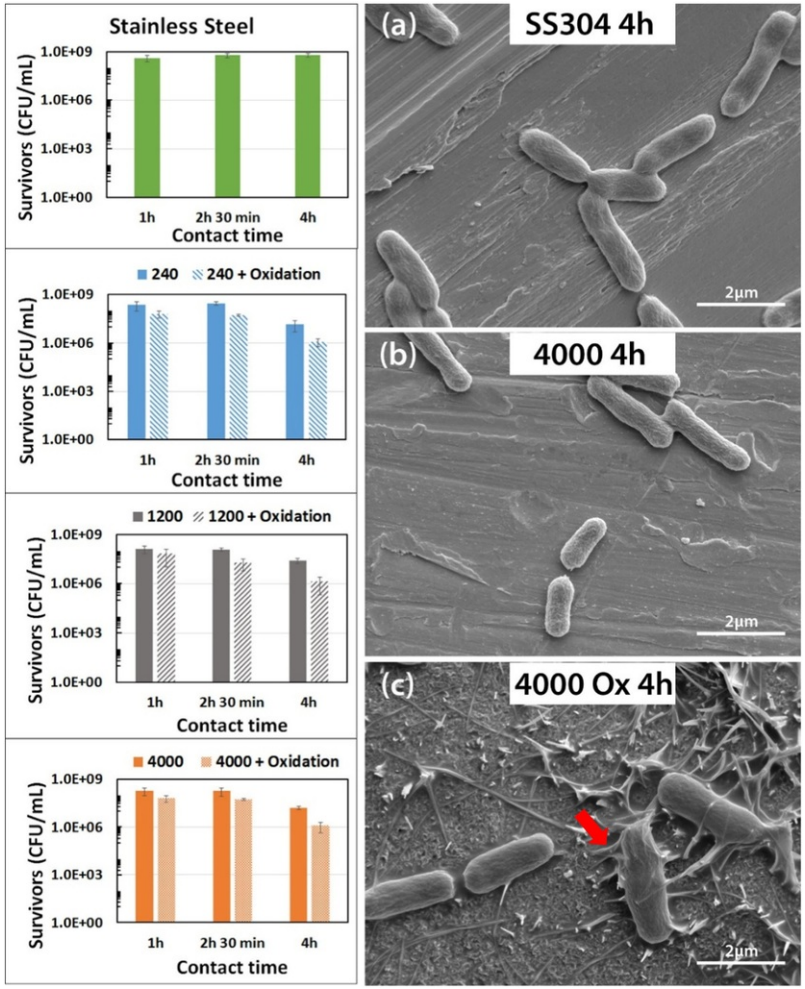

~~Fig. 6.~~Fig. 6 Survival rate values of *E. coli* on steel and the ground samples before and after oxidation for 1, 2.5 and 4 h of contact time. SEM images of *E. coli* cells deposited on (a) SS314, (b) 4000 as-cast and (c) 4000 oxidized after 4 h of contact time (fimbriae indicated by arrow).

alt-text: Fig. 6

When *E. coli* was exposed to the as-cast samples of different roughness (240, 1200 and 4000 grit) the apparent killing rates were equivalent. Similar values of bacteria were recovered after 1 h and 2.5 h of contact (~2~~×~~×10^8 CFU/mL) but a significant reduction in recovered bacteria (~1.5~~×~~×10^7 CFU/mL) were observed after 4 h, which is consistent with those previously observed in other metallic glass composites [3]. This suggests that the surface roughness had a limited effect on antimicrobial activity. A similar trend can be noticed in all oxidized samples, however, they exhibit lower survival values (6~~×~~×10^7 CFU/mL after 1 h, 3~~×~~×10^7 CFU/mL after 2.5 h and 8~~×~~×10^5 CFU/mL after 4 h). Importantly, although the concentration of Cu in the BMGC is slightly higher (55 at. %) than for the CuO outer layer, which is 50 at. %, the antimicrobial properties of the surface after oxidation is higher. This difference could be partly attributed to the microstructure of CuO (Figs. 2c and ~~Fig.~~ 6c), consisting of multiple finely dispersed needles of ~~less than~~ ≤1 µm long. Fine microstructures promote the diffusion of Cu^+ and Cu^{++} since they contain a large volume fraction of grain boundaries [5], which are easy paths for the Cu ions to diffuse to the surface. However, other factors are suggested to contribute as hereafter commented. Contrary to previous reports, where the antimicrobial effect of copper oxide compared to the substrate was attributed to differences in composition and medium, the results presented here indicate that the surface fine and needle shape microstructure has a key role, which explains the enhanced antimicrobial performance of the oxidized sample, even though it is 5 at. % poorer in copper than the substrate. The difference in antimicrobial activity, counted as the number of surviving CFU, between the bulk and oxidized samples increases as the contact time increases (Fig. 6): 5 % (1 h), 10 % (2 h30 min) and 30 % (4 h) irrespective of the surface roughness (240, 1200 or 4000 grit). This trend is consistent with the kinetics of a diffusive process.

SEM images of the bacteria deposited on stainless steel (Fig. 6a) reveal obvious morphological variations. Some of the bacteria are observed to be generating structures that project from their surface (arrow Fig. 6c), which are very likely to represent fimbriae or pili (i.e., functionally related structures that are implicated in bacterial adhesion). These structures, of which there are several subtypes, are subject to complex genetic regulatory pathways including phase variation, which generates a variety of bacteria with different profiles of gene expression [21]. These variations are thought to improve the likelihood of bacteria to colonize new environments. In fact, their appearance (Fig. 6c) may suggest that a minor subset of variants is able to bind more avidly, and thus frequently, to the oxidized surface than to the surface of the non-oxidized materials. However, bacterial changes in morphology from exposure to the surfaces are very small (i.e., there is no apparent rupture of the envelope with cytosol leakage) [22]. Bacteria deposited on the 4000 as-cast sample (Fig. 6b) show a similar undamaged envelope to that observed in the cells deposited on steel, however, those deposited on the 4000 oxidized alloy (Fig. 6c) maintain the typical rod shape but appear thicker. Similar morphological changes have been suggested to be an indicator of *E. coli* bacteria damage [19,20,23].

Fig. 6c also revealed the presence of a layer on top of the *E. coli* cells which is near the copper oxide needles (arrow in Fig. 6c). This needle shaped phase was present in the oxidized samples before the antimicrobial tests (Fig. 2c), but they developed further during the antimicrobial tests performed in wet conditions, i.e. with liquid media always in contact with the sample. EDX measurements indicated a compositional range between $O_{53.0}Cu_{47.0}$ and $O_{56.5}Cu_{43.5}$ at. % and, therefore may be attributed to CuO. The material coating these cells may be escaping cellular contents from lysed cells, however the cells appear to be relatively intact. Alternatively, this material could be secreted polysaccharide, similar to that secreted as a response to stress [24] suggests a protective role triggered by envelope stresses. It is possible that the production of this layer is activated by stimulation of the mechanosensitive channels, due to the increase of pressure on the cell exerted by the needles [25].

The consistency in the number of recovered bacteria despite modification of the surface roughness is of interest, since other authors have shown that roughness has an effect on the wettability and bacterial attachment [25], further affecting biofilm formation [26,27] and antimicrobial performance [28]. The main difference can be observed between the as-cast and oxidized samples. The needle shaped material present in the latter may have exerted a mechanical force on the *E. coli* cells (Fig. 6c), changing the cell membrane curvature and triggering the mechanosensitive channels present in the plasma membrane of the cells [29]. These structures serve as adaptable sensors which must sense and respond to changes in external and internal mechanical forces so mechanical stimuli can lead to the opening of such channels. The Mechanosensitive channel of Small conductance (MscS) and Mechanosensitive channel of Large conductance (MscL) in *E. coli* cells are non-selective, and while MscS shows a preference to chlorine over potassium, MscL are permeable to any anion or cation [30]. These mechanosensors have a threshold tension for activation of ~6.0 and ~12.0 mN/m respectively [31–33] and are sensitive to changes in membrane morphology. The local increase in stress and subsequent change in cell membrane curvature driven by the observed CuO phase may have caused the triggering of such channels, altering the cell envelope permeability and effectively increasing the migration of copper ions into the cell. Copper ions would then interfere with the homeostasis of other metals, damage DNA and produce Reactive Oxygen Species (ROS) which modify proteins, lipids and nucleic acids [34–36], thus causing the death of *E. coli* cells without visible disruption of the cell wall. On the other hand, due to the lack of CuO needles in the as-cast samples, the mechanosensitive ion channel opening would be absent, in addition, the microstructure is coarser, which might explain the lower antimicrobial behavior of the as cast alloy [20,23]. Consequently, the fine microstructure of copper rich needles, as well as, variations in cell membrane permeability would account for the higher antimicrobial behavior of the oxidized samples.

Besides superficial changes, the oxidation state of the copper ions (Cu^{+1} and/or Cu^{+2}) may have an influence on the antimicrobial properties, but this point is debated. On the one hand, Cu^{+1} ions have been reported to be less effective in bacterial killing than Cu^{2+} ions, since the latter possess high affinity to phosphorus- and sulphur-containing compounds present inside cells [37–39]. In contrast, Hans et al. [7] have shown that Cu_2O is more toxic than CuO suggesting that Cu^{+1} can be more antimicrobial than Cu^{+2}. In summary, the antimicrobial performance is a multifactorial and complex process that cannot be explained solely in terms of the composition.

To assess a wider range of Cu concentrations and their effect on *E. coli* morphology, including when the bacteria rupture, Minimum Inhibitory Concentration (MIC) tests (Fig. 7) were carried out by following the CLSI approved standard M07-A9 [37]. It was found that 3.5 mM of copper (II) chloride dihydrate ($CuCl_2 \cdot 2(H_2O)$) completely inhibited the growth of the bacterium, as evidenced by the lack of turbidity in the corresponding test tubes, which agreed with the reports of Santo et al. [38] and Ruparelia et al. [39]. These strong correlations with the sensitivity observed with other strain of *E. coli* indicate that our strain is adequately sensitive for this study. SEM images (Fig. 7) of bacteria treated with different Cu concentrations (i.e. 0.1 mM, 3.5 mM and 5 mM) of copper (II) chloride dihydrate ($CuCl_2 \cdot 2(H2O)$) deposited on stainless steel show progressive envelope damage as the concentration of copper ions increases. For the lowest concentration (0.1 mM, Fig. 7a), bacteria do not display any apparent damage, while some cells can be seen in the middle of cell division, which is consistent with their continued growth and tolerable concentration of copper ions. At 3.5 mM copper (II) chloride (Fig. 7b), significant changes in bacterial morphology are evident with some the cells displaying a complete loss of structural integrity (i.e. lysis). The bacteria displaying an apparently “undamaged” envelope appear swollen compared to *E. coli* cells observed in lower $CuCl_2 \cdot 2(H_2O)$ concentrations. The lack of growth in the sample after inoculation indicates that these cells are incapable of proliferation and are likely dead. Finally, SEM analysis of cells exposed to 5 mM of the copper compound (Fig. 7c) revealed widespread and complete destruction of the cell envelope where all bacteria have lost their structural integrity. Only a few remnants from an organic substance similar to an amalgam of cell membrane remains (see arrow in Fig. 7c), suggesting the complete elimination of *E. coli* cells.

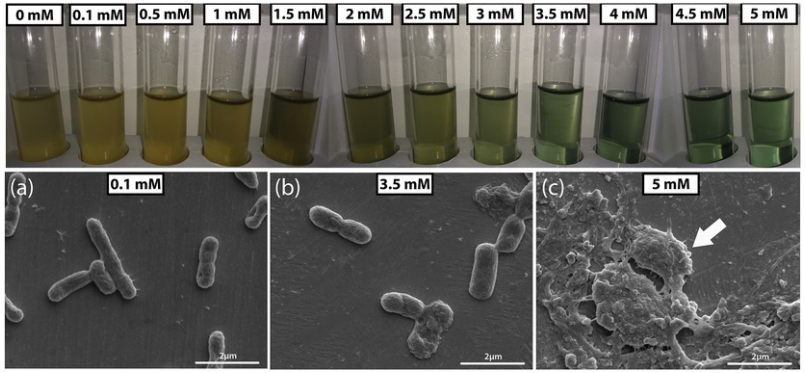

~~Fig. 7.~~Fig. 7 Minimum Inhibitory Concentration tests as described in CLSI M07-A9 standard and Secondary Electron images of *E. coli* treated with (a) 0.1 mM, (b) 3.5 mM and (c) 5.0 mM deposited on stainless steel.

alt-text: Fig. 7

~~3.3.~~3.3 Cu ion diffusion and antimicrobial map

To further analyze the correlation between Cu ion diffusion and antimicrobial properties, the number of Cu ions diffused from the samples after 1, 2.5 and 4 h of contact with LB broth was measured using ICP. The number of Cu ions in the as-cast samples rises as the time contact increased (60.2 ± 60.9 ppb for 1 h, 167.4 ± 64.0 ppb for 2.5 h and 262.0 ± 103.2 ppb for 4 h). A similar trend was observed for the oxidized samples, however, the concentration of Cu is five times higher for the same contact time (320.1 ± 60.9 ppb for 1 h, 992.1 ± 450.0 ppb for 2.5 h and 1232.0 ± 368.9 ppb for 4 h). These values are much higher than those observed by Chu et al. [40] for amorphous Zr–Cu–Ni–Al thin films. The number of copper ions released from the surface ranged from 35 ppb to 11,990 ppb after 1 day and 21 days of contact time, respectively. The values obtained for our samples are much higher than the 35 ppb obtained by Chu et al. [40]. This can be correlated with the increase in Cu diffusion paths due to the presence of grain boundaries in the BMGC for the as-cast and oxidized conditions [41]. The rise in Cu ions could be responsible for the reduction in *E. coli* cells as shown in Fig. 6, while, at the same time, the higher number of copper ions measured in the oxidized samples agrees with the higher antimicrobial performance displayed by these alloys.

It is interesting to notice the similarities and differences between the MIC and ICP results. The maximum number of Cu ions measured was detected for the oxidized sample after 4 h (1232.0 ± 368.9 ppb ≈ 0.02 mM). Using the results obtained in the MIC tests (Fig. 6), all *E. coli* cells should remain alive with undamaged envelopes. However, the number of viable cells is reduced, as shown in Fig. 6, indicating a relatively high antimicrobial activity. This apparent contradiction can be attributed to the differences between both experiments. In the MIC tests, a set amount of copper was inoculated into each test tube, while the concentration of Cu in the antimicrobial tests increases continuously. Dead cells will act as reservoirs of Cu ions, diminishing the concentration of Cu, which can affect other cells in the MIC tests. In contrast, the copper absorbed by these cells is continuously renewed in the antimicrobial tests, preventing the survival of other cells. It should be mentioned that the morphological features shown in the antimicrobial tests (Fig. 6) are agree with the low concentrations of Cu in the MIC tests (Fig. 7a). This suggests that the initial steps during the removal of *E. coli* cells in contact with Cu-rich samples are dominated by internal damage rather than degradation of the external envelope.

Over the years, the development of new antimicrobial surfaces has been driven by the accumulation of empirical evidence. This approach, however, is time-consuming and may require use of a large number of samples. To tackle this issue, we have used the previous experimental results for the unoxidized Cu-based bulk metallic glass to develop an “antimicrobial map” (Fig. 8). This map correlates the number of Cu ions released over contact time with the morphology of bacteria analyzed by SEM in order to assess the damage. The map consists of four different regions <60% red, 50-~~-~~60% blue, 60-~~-~~99% green and >99% white representing the percentage of CFU/mL surviving [42] a copper ion concentration for a set amount of time, as well as, the commonly cited 3 log reduction stated in JIS Z 2018:2010 [43]. These estimated boundary lines are expected to be more precisely defined as more experimental points of data are collected in the future. The position of the dashed line indicates that only after ~~more than~~> ~~four hours~~4 h the analyzed BMG composite can reach the desired $\log_{10}$ reduction, thus, the metallic alloy cannot be labelled as antimicrobial. Only materials which release enough Cu ions in 1 ~~hour~~h will comply with this standard and, as a result, a product could be considered as antimicrobial or not only by measuring the Cu ions released by the material. These maps will be defined for a bacterium (i.e. *E. coli K12*) and a culture broth (i.e. LB broth), due the influence of these parameters in the corrosion and subsequent release of Cu ions [44–48]. Lines of constant antimicrobial activity or percentage reduction (isolines) can be either horizontal or change as contact time increases. In cases where the release of copper is not enough to completely inhibit the growth of bacteria, cells will undergo division, leading to concave isolines, while quick release of Cu ions may be related with convex isolines. Consequently, low percentage reductions will be concave, while higher isolines will be convex. On the other hand, boundary conditions indicate that for time limits near the origin of the map, the quantity of Cu ions necessary to achieve a set antimicrobial activity must be higher. Thus, all isolines should have a limit for times near zero tending to infinite, which quickly stabilizes in convex or concave curves. To illustrate one use of this map, Fig. 8 shows an estimation of the Cu ions necessary to be released by our BMG composite to comply with the limits imposed by the United States Food and Drug Administration (3 $\log_{10}$ reduction in 1 h) [1].

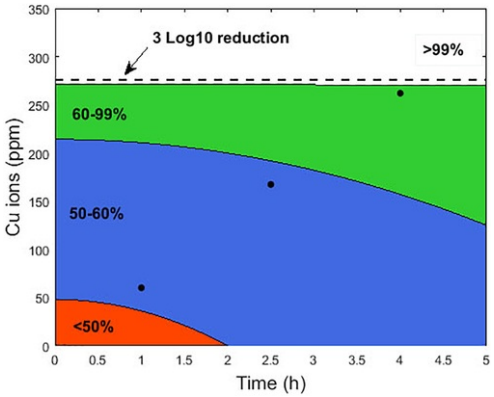

~~Fig. 8.~~**Fig. 8** Sketch of antimicrobial map for *E. coli K12* in LB broth for the as-cast $Cu_{55}Zr_{40}Al_5$ BMGC.

alt-text: Fig. 8

This attempt to sketch antimicrobial maps has certain constraints that need to be addressed in the future as more points of data are collected and the boundary lines redefined. However, this map can provide a rapid estimation of the antimicrobial efficiency that can help select the most suitable antimicrobial material.

~~4.~~4 Conclusions

The contact killing efficiency of $Cu_{55}Zr_{40}Al_5$ at. % BMGC with different roughness (240, 1200 and 4000 SiC grit) and after oxidation has been compared using *E. coli* in wet conditions through Luria-Bertani medium. We have shown that, contrary to other reports, the roughness does not have an effect on the antimicrobial ~~behaviour~~behavior, however, formation of an outer CuO layer upon heat treatment increases the antimicrobial performance. This was not expected since the CuO layer is more poor in Cu (50 at. %) than the BMGC substrate (55 at. %). The antimicrobial performance is a multifactorial and complex process that cannot be explained in term of the composition. The performance is attributed to the fine microstructure and shape of the needles present in the CuO layer. This involves a large volume fraction of interphases that promotes the diffusion of Cu ions and also the needle shape oxide can trigger mechanosensitive channels and thus promote the migration of copper ions into the cell. Additionally, an antimicrobial map compiled from available relevant experimental data has been proposed. This is expected to be useful in guiding future material selection, especially when the accuracy of the map improves as more experimental data points are added in the future. This work shows that surface engineering through oxidation of $Cu_{55}Zr_{40}Al_5$ at. % BMGC enables to enhance the antimicrobial performance and therefore it is a promising strategy for development of antimicrobial surfaces in the healthcare sector.

Acknowledgements

V. M. Villapún, L. G. Dover and S. González acknowledge research support from Northumbria University.

References

[1] V.M. Villapún, L.G. Dover, A. Cross and S. González, Antibacterial metallic touch surfaces, *Materials* **9**, 2016, 736.

[2] NHS, Infection: ~~p~~Prevention and ~~c~~Control of ~~h~~Healthcare ~~a~~Associated ~~i~~Infections in ~~p~~Primary and ~~c~~Community ~~c~~Care, Costing ~~s~~Statement, 2012.

[3] V.M. Villapún, F. Esat, S. Bull, L.G. Dover and S. González, Tuning the ~~M~~mechanical and ~~A~~antimicrobial ~~P~~performance of a Cu-~~B~~based ~~M~~metallic ~~G~~glass ~~C~~composite through ~~C~~cooling ~~R~~rate ~~C~~control and ~~A~~annealing, *Materials* **10**, 2017, 506.

[4] L. Huang, E.M. Fozo, T. Zhang, P.K. Liaw and W. He, Antimicrobial behavior of Cu-bearing Zr-based bulk metallic glasses, *Mater. Sci. Eng. C* **39**, 2014, 325–329.

[5] H.B. Aaron and F. Weinberg, Preferential diffusion along interphase boundaries, ~~*Acta Metallurgica*~~*Acta Metall.* **20**, 1972.

[6] A. International, Surface Engineering for Corrosion and Wear Resistance, 2001, ASM International.

[7] S. González, E. Pellicer, S. Suriñach, M.D. Baró, E. García-Lecina and J. Sort, Effect of thermally-induced surface oxidation on the mechanical properties and corrosion resistance of Zr60Cu25Al10Fe5 bulk metallic glass, *Sci. Adv. Mater.* **6**, 2014, 27–36.

[8] M. Hans, A. Erbe, S. Matthews, Y. Chen, M. Solioz and F. Mücklich, Role of copper oxides in contact killing of bacteria, *Langmuir* **29**, 2013, 16160–16166.

[9] M. Taran, M. Rad and M. Alavi, Antibacterial activity of copper oxide (CuO) nanoparticles biosynthesized by Bacillus sp. FU4: ~~O~~optimization of ~~E~~experiment design, *Pharm. Sci.* **23**, 2017, 198–206.

[10] K. Gold, B. Slay, M. Knackstedt and A.K. Gaharwar, Antimicrobial activity of metal and metal-oxide based nanoparticles, *Adv. Ther.* **1**, 2018, 1700033.

[11] C.P. Adams, K.A. Walker, S.O. Obare and K.M. Docherty, Size-dependent antimicrobial effects of novel palladium nanoparticles, *PLoS ONE* **9**, 2011, e85981.

[12] J. Hasan and K. Chatterjee, Recent advances in engineering topography mediated antibacterial surfaces, *Nanoscale* **7**, 2015, 15568–15575.

[13] N.J. Shirtcliffe, G. McHale, S. Atherton and M.I. Newton, An introduction to superhydrophobicity, ~~*Adv. Colloid Interface Sci.*~~*Adv. Colloid Interf. Sci.* **161**, 2010, 124–138.

[14] P.A. Wayne, CLSI Methods for Dilution Antimicrobial Susceptibility Tests for Bacteria That Grow Aerobically, CLSI ~~d~~Document M07—A9 32, 2012.

[15] E.R. Fischer, B.T. Hansen, V. Nair, F.H. Hoyt and D.W. Dorward, Scanning ~~E~~electron ~~M~~microscopy, *Curr. Protoc. Microbiol.* **25**, 2012, B:2B.2:2B.2.1–2B.2.47.

[16] C.Y. Tam and C.H. Shek, Oxidation behavior of Cu 60Zr 30 Ti 10 bulk metallic glass, *J. Mater. Res.* **20**, 2005, 1396–1403.

[17] K. Asami, M. Kikuchi and K. Hashimoto, An auger electron spectroscopic study of the corrosion behavior of an amorphous Zr40Cu60 alloy, *Corros. Sci.* **39**, 1997, 95–106.

[18] C.Y. Tam, C.H. Shek and W.H. Wang, Oxidation behaviour of a Cu-Zr-Al bulk metallic glass, *Rev. Adv. Mater. Sci.* **18**, 2008, 107–111.

[19] M. Schaechter, The Desk Encyclopedia of Microbiology, Sevier, San Diego, CA, USA2009.

[20] M. Raffi, S. Mehrwan, T.M. Bhatti, J.I. Akhter, A. Hameed, W. Yawar and M.M. ul Hasan, Investigations into the antibacterial behavior of copper nanoparticles against Escherichia coli, *Ann. Microbiol.* **60**, 2010, 75–80.

[21] J.H. N. and D.L. G., Switches, cross-talk and memory in Escherichia coli adherence, ~~*Journal of Medical Microbiology*~~*J. Med. Microbiol.* **53**, 2004, 585–593.

[22] Y. Liu, J. Padmanabhan, B. Cheung, J. Liu, Z. Chen, B.E. Scanley, D. Wesolowski, M. Pressley, C.C. Broadbridge, S. Altman, U.D. Schwarz, T.R. Kyriakides and J. Schroers, Combinatorial development of antibacterial Zr-Cu-Al-Ag thin film metallic glass, *Sci. Rep.* **6**, 2016, 26950.

[23] U. Bogdanović, V. Lazić, V. Vodnik, M. Budimir, Z. Marković and S. Dimitrijević, Copper nanoparticles with high antimicrobial activity, *Mater. Lett.* **128**, 2014, 75–78.

[24] M. Ionescu and S. Belkin, Overproduction of exopolysaccharides by an Escherichia coli K-12 rpoS mutant in response to osmotic stress, *Appl. Environ. Microbiol.* **75**, 2009, 483–492.

[25] E.E. Mann, D. Manna, M.R. Mettetal, R.M. May, E.M. Dannemiller, K.K. Chung, A.B. Brennan and S.T. Reddy, Surface micropattern limits bacterial contamination, ~~*Antimicrob. Resist. Infect. Contro*~~*Antimicrob Resist Infect Contro.* **28**, 2014, 1–8.

[26] M.F. Copeland and D.B. Weibel, Bacterial swarming: a model system for studying dynamic self-assembly, *Soft Matter* **5**, 2009, 1174–1187.

[27] A. Taubert, J.F. Mano and J.C. Rodríguez-Cabello, Biomaterials ~~s~~Surface ~~s~~Science, 2013, John Wiley & Sons.

[28] H.W. Chen, K.C. Hsu, Y.C. Chan, J.G. Duh, J.W. Lee, J.S.C. Jang and G.J. Chen, Antimicrobial properties of Zr–Cu–Al–Ag thin film metallic glass, *Thin Solid Films* **561**, 2014, 98–101.

[29] E.S. Haswell, R. Phillips and D.C. Rees, Mechanosensitive channels: what can they do and how do they do it?, *Structure* **19**, 2011, 1356–1369.

[30] B. Martinac, Y. Saimi and C. Kung, Ion channels in microbes, *Physiol. Rev.* **88**, 2008, 1449–1490.

[31] S. Sukharev, Purification of the small mechanosensitive channel of Escherichia coli (mscS): the subunit structure, conduction, and gating characteristics in liposomes, *Biophys. J.* **83**, 2002, 290–298.

[32] S.I. Sukharev, W.J. Sigurdson, C. Kung and F. Sachs, Energetic and spatial parameters for gating of the bacterial large conductance mechanosensitive channel, MscL, *J. Gen. Physiol.* **113**, 1999, 525–540.

[33] R. Peyronnet, D. Tran, T. Girault and J.M. Frachisse, Mechanosensitive channels: feeling tension in a world under pressure, ~~*Front. Plant. Sci.*~~*Front. Plant Sci.* **5**, 2014, 558.

[34] E. Zhang, L. Zheng, J. Liu, B. Bai and C. Liu, Influence of Cu content on the cell biocompatibility of Ti–Cu sintered alloys, *Mater. Sci. Eng. C* **46**, 2015, 148–157.

[35] O.I. Aruoma, B. Halliwell, E. Gajewski and M. Dizdaroglu, Copper-ion dependent damage to the bases in DNA in the presence of hydrogen-peroxide, *J. Biol.* **273**, 1991.

[36] L. Banci, I. Bertini, F. Cantini and S. Ciofi-Baffoni, Cellular copper distribution: a mechanistic systems biology approach, *Cell. Mol. Life Sci.* **67**, 2010, 2563–2589.

[37] Y.J. Park, Y.H. Song, J.H. An, H.J. Song and K.J. Anusavice, Cytocompatibility of pure metals and experimental binary titanium alloys for implant materials, *J. Dent.* **41**, 2013, 1251–1258.

[38] A. Shedle, P. Samorapoompichit, X.H. Rausch-Fan, A. Franz, W. Fureder, W.R. Sperr, W. Sperr, A. Ellinger, R. Slavicek, G. Boltz-Nitulescu and P. Valent, Response of L-929 fibroblasts, human gingival fibroblasts, and human tissue mast cells to various metal cations, *J. Dent. Res.* **74**, 1995, 1513–1520.

[39] A. Yamamoto, R. Honma and M. Sumita, Cytotoxicity evaluation of 43 metal salts using murine fibroblasts and osteoblastic cells, *J. Biomed. Mater. Res.* **39**, 1998, 331–340.

[40] J.H. Chu, J. Lee, C.C. Chang, Y.C. Chan, M.L. Liou, J.W. Lee, J.S.C. Jang and J.G. Duh, Antimicrobial characteristics in ~~C~~cu-containing Zr-based thin film metallic glass, *Surf. Coat. Technol.* **259**, 2014, 87–93.

[41] V.K. Champagne and D.J. Helfritch, A demonstration of the antimicrobial effectiveness of various copper surfaces, *J. Biol. Eng.* **7**, 2013, 1–6.

[42] U.S.E.P, Agency, 2016, EPA.

[43] J.S. Association, in, Akasaka, Minato-ku, Tokyo, 2010.

[44] H.B. Lu, Y. Li and F.H. Wang, Corrosion behavior and porous structure formation of sputtered ~~C~~cu–Zr nanostructured films, *J. Alloys Compd.* **465**, 2008, 139–144.

[45] H.B. Lu, L.C. Zhang, A. Gebert and L. Schultz, Pitting corrosion of Cu–Zr metallic glasses in hydrochloric acid solutions, *J. Alloys Compd.* **462**, 2008, 60–67.

[46] J. Tang, Q. Zhu, Y. Wang, M. Apreutesei, H. Wang, P. Steyer, M. Chamas and A. Billard, Insights on the ~~R~~role of ~~C~~copper ~~A~~addition in the ~~C~~corrosion and ~~M~~mechanical ~~P~~properties of ~~B~~binary Zr-Cu ~~M~~metallic ~~G~~glass ~~C~~coatings, *Coatings* **7**, 2017, 223.

[47] B. Little, P. Wagner and F. Mansfeld, Microbiologically influenced corrosion of metals and alloys, *Int. Mater. Rev.* **36**, 1991, 253–272.

[48] L. Huang, D. Qiao, B.A. Green, P.K. Liaw, J. Wang, S. Pang and T. Zhang, Bio-corrosion study on zirconium-based bulk-metallic glasses, *Intermetallics* **17**, 2009, 195–199.

Graphical abstract

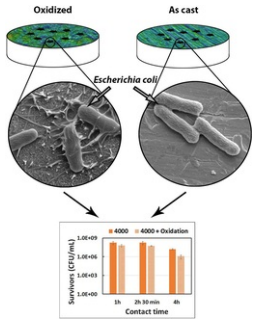

alt-text: Unlabelled Image

Highlights

- Influence of surface roughness and oxidation against *E. coli*
- Antimicrobial performance is a multifactorial and complex process.
- Oxidation of $Cu_{55}Zr_{40}Al_5$ at. % alloy enables to enhance the antimicrobial performance.
- Roughness change from 240 to 4000 grit does not have antimicrobial effect.

Queries and Answers

Query:

Your article is registered as a regular item and is being processed for inclusion in a regular issue of the journal. If this is NOT correct and your article belongs to a Special Issue/Collection please contact s.vikram@elsevier.com immediately prior to returning your corrections.

Answer: Yes

Query:

Please confirm that given names and surnames have been identified correctly and are presented in the desired order, and please carefully verify the spelling of all authors' names.

Answer: Yes

Query:

The author names have been tagged as given names and surnames (surnames are highlighted in teal color). Please confirm if they have been identified correctly.

Answer: Yes

Query:

Please check whether the designated corresponding author is correct, and amend if necessary.

Answer: Yes, It is correct.

Query:

Both the lowercase Latin letter "l" and the uppercase Latin letter "L" are used to represent the unit "liter" or its variations (e.g., milliliter, microliter) in the text. For consistency, kindly modify these occurrences so that only one format is used throughout the article.

Answer: It is fine.

Query:

Have we correctly interpreted the following funding source(s) and country names you cited in your article: "Northumbria University".

Answer: Yes